J. Korean Soc. Ind. Appl. Math. Vol.23, No.3, 211–236, 2019 http://doi.org/10.12941/jksiam.2019.23.211

NUMERICAL COUPLING OF TWO SCALAR CONSERVATION LAWS BY A RKDG METHOD

NASRIN OKHOVATI[1] AND MOHAMMAD IZADI[2]

[1]DEPARTMENT OF MATHEMATICS, KERMAN BRANCH, ISLAMIC AZAD UIVERSITY, KERMAN, IRAN.
Email address: diamand_2010@yahoo.com

[2]DEPARTMENT OF APPLIED MATHEMATICS, FACULTY OF MATHEMATICS AND COMPUTER, SHAHID BAHONAR UNIVERSITY OF KERMAN, KERMAN, IRAN.
Email address: izadi@uk.ac.ir

ABSTRACT. This paper is devoted to the study and investigation of the Runge-Kutta discontinuous Galerkin method for a system of differential equations consisting of two hyperbolic conservation laws. The numerical coupling flux which is used at a given interface ($x = 0$) is the upwind flux. Moreover, in the linear case, we derive optimal convergence rates in the L_2-norm, showing an error estimate of order $\mathcal{O}(h^{k+1})$ in domains where the exact solution is smooth; here h is the mesh width and k is the degree of the (orthogonal Legendre) polynomial functions spanning the finite element subspace. The underlying temporal discretization scheme in time is the third-order total variation diminishing Runge-Kutta scheme. We justify the advantages of the Runge-Kutta discontinuous Galerkin method in a series of numerical examples.

1. INTRODUCTION

Recent years have seen a growing interest in developing numerical algorithms for the coupling of hyperbolic equations due to their numerous applications, specially in the modeling of complex systems. Actually, it may first occur in the framework of the modeling of two-phase flow in porous media. The coupling of two conservation laws was first addressed and numerically analyzed by Godlewski and Raviart, in the case of scalar conservation laws [1] and was continued in the case of systems of conservation laws [2]. The study of coupling phenomenon has now been considered via different models that naturally appears for example in an increasing number of problems of fluid mechanics. Among others, we emphasize the case of two Euler systems for gas dynamics with two different equations of state [3] as well as modeling coupled systems of different dimensions [4], the homogeneous models for two-phase flows [5],

Received by the editors July 8 2019; Revised September 12 2019; Accepted in revised form September 14 2019; Published online September 25 2019.
2000 *Mathematics Subject Classification.* 35L65, 65M60, 65M12, 65N40.
Key words and phrases. Conservation laws, Discontinuous flux, Discontinuous Galerkin methods, Coupling equations, Error estimates.
[2] Corresponding author.

and the coupling of multiphase flow [6]. For an overview of some recent results devoted to the coupling problems we refer the reader to [7] and the references therein.

The main goal of this paper is to devise, analyze, and implement the Runge-Kutta discontinuous Galerkin method (RKDG) for the solution of the interface problem in a system of two different partial differential equations. More precisely, we consider the following coupling of two conservation laws in one dimension: Find $u : (x,t) \in \mathbb{R} \times \mathbb{R}_+ \longmapsto u(x,t) \in \mathbb{R}$ such that

$$\begin{cases} u_t + f_R(u)_x &= 0, \quad x > 0, \quad t > 0, \\ u_t + f_L(u)_x &= 0, \quad x < 0, \quad t > 0, \end{cases} \tag{1.1a}$$

with initial condition

$$u(x,0) = u_0(x), \qquad x \in \mathbb{R}, \tag{1.1b}$$

where $u_0 : \mathbb{R} \longrightarrow \mathbb{R}$ is a given function and $f_\alpha : \mathbb{R} \longrightarrow \mathbb{R}$, for $\alpha = L, R$, denote two *smooth* functions. Due to the fact that imposing the initial data $u_0(x)$ at time $t = 0$ does not suffice for well-posedness of two boundary value problems on each half-space $x < 0$ and $x > 0$, these equations are supplemented by a suitable "continuity condition" which is also referred to as a "coupling condition" at the fixed interface $x = 0$:

$$\Phi_L(u(0^-,t)) = \Phi_R(u(0^+,t)), \quad t > 0, \tag{1.1c}$$

to be compatible with the initial condition u_0. Here Φ_α, for $\alpha = L, R$ are two given smooth functions to be specified below and $u(0^\pm,t) = \lim_{s \longrightarrow 0^\pm} u(x+s,t)$ are called the left and right traces. Different approaches for treating a coupling condition can be defined through specifying Φ_α for $\alpha = L, R$. For example, by selecting $\Phi_\alpha = Id$ one expects the continuity of the solution u at the interface, without imposing the conservativity of the coupled model, see [1, 2]. This approach is called "state coupling".

In contrast to the state coupling, one may consider "flux coupling". In the flux coupling approach with $\Phi_\alpha = f_\alpha$ for $\alpha = L, R$, i.e., $f_L(u(0^-,t)) = f_R(u(0^+,t)), t > 0$, one expects the continuity of the fluxes and the conservation of the unknown at $x = 0$. Indeed, such continuity condition is natural in several setting and comes from the fact that two half-space equations (1.1a) can be seen as a single equation with an unique discontinuous flux function (see equation (2.1) below). The flux coupling method has received a considerable attention over the past decade from both theoretical and numerical point of views, see for instance [8, 9, 10, 11, 12], and [13]. In this work, our strategy for treating the coupling equations (1.1a)-(1.1c) is relied on the latter approach.

For last decades, the technique of discontinuous Galerkin (DG) investigated as an higher-order accurate scheme for treating differential equations specially for those problems with hyperbolic nature and developing discontinuities. The DG methods can be viewed as a combination of both finite element methods (FEMs), allowing for discontinuous discrete function, and finite volume methods (FVMs), with more than one degree of freedom per mesh element. This extended scheme offers great opportunities relative to traditional FEMs when used to discretized hyperbolic problems. The main benefits of the DG methods can be summarized in terms of: accuracy; since the local polynomial order can be adapted according to an estimation

of the error, flexibility; since neighboring cells are only coupled weakly, and parallelizability, since there is a simple communication pattern between elements that makes it useful for parallel computation and also the amount of communication does depend on the polynomial degree.

The first DG method was introduced in 1973 by Reed and Hill [14], for numerically solving neutron transport, i.e. a time independent linear hyperbolic equation. As the first error analysis of the DG method for this problem, LeSaint and Raviart [15] proved that the L_2-norm of the error is $\mathcal{O}(h^k)$ when polynomials of degree k are used on a mesh of size h. The theory of discontinuous Galerkin schemes was then generalized to linear hyperbolic problems by Johnson and Pitkäranta [16] by introducing mesh-dependent norms and were able to derive a priori error estimates of order $\mathcal{O}(h^{k+\frac{1}{2}})$. Peterson [17] numerically confirmed that this estimate is actually sharp for the most general situation. In 1988, Richter [18] obtained the optimal order of convergence of $\mathcal{O}(h^{k+1})$. DG methods were extended to nonlinear hyperbolic conservation laws by Cockburn, Hou and Shu [19] who developed a local projection strategy to provide nonlinear stability.

The type of DG methods we will consider in this paper, the approximate solution is sought in a piecewise discontinuous polynomial space with respect to the spatial variables and appropriate explicit Runge-Kutta method is applied in the time-marching. To achieve stability, the nonlinearly stable high order Runge-Kutta time discretization [20] is used, were first developed for conservation laws containing first derivatives by Cockburn and Shu [21, 22]. For a detailed description of the method as well as its implementation and applications, consult [23, 24] and the references cited therein for more information on DG methods.

In this paper we go beyond the classical finite difference and finite volume schemes for numerical treatments of the coupling problems as investigated by many papers, see a recent survey [7] and [25]. We take a further step towards proposing a numerical method of coupling in the frame of DG schemes which is a combination of both FV and FE. Roughly speaking, we are interested to investigate the performance of the RKDG method by extending the work in the above references, when applied to the system of two hyperbolic conservation laws (1.1). The main focus is to implement, derive a priori error estimate of $\mathcal{O}(h^{k+1})$ theoretically, and justify this fact numerically.

The contents of this paper is structured as follows. In Section 2, we introduce notations, definitions, make some assumptions, and present auxiliary results which will be used in the subsequent sections. Section 3 is devoted to the formulation of the DG method together with a detailed description of the numerical coupling flux function at the interface. In Section 4, we state a cell entropy inequality for the corresponding proposed DG scheme. The optimal error estimate in the linear case and with the specially chosen numerical flux is given in Section 5. Section 6 provides a detailed exposition of numerical implementation of the RKDG scheme for the linear coupled problem based upon Legendre polynomials. In Section 7, we demonstrate the capabilities of the RKDG method and verify the theoretical results by performing numerical experiments. A comparison also has been presented between the RKDG scheme and the classical finite volume methods. The paper ends with some conclusions in Section 8.

2. PRELIMINARIES

In this section we introduce some notations and definitions to be used later in the paper and also present some auxiliary results. To start, we begin by introducing an auxiliary function, i.e., the Heaviside step function

$$\gamma(x) := \begin{cases} 0, & x > 0, \\ 1, & x < 0, \end{cases}$$

which allows us to rewrite the two half-space equations (1.1a) into a single equation. Letting the flux function

$$F(\gamma(x), u) := \gamma(x) \cdot f_L(u) + (1 - \gamma(x)) \cdot f_R(u), \tag{2.1}$$

which is discontinuous with respect to the spatial variable x, one can reformulate (1.1a)-(1.1b) in the following compact form

$$\begin{cases} u_t + [F(\gamma(x), u)]_x &= 0, & (x,t) \in \Omega := \mathbb{R} \times \mathbb{R}_+ \\ u(x,0) &= u_0(x), & x \in \mathbb{R}. \end{cases} \tag{2.2}$$

It is well-known that even for a smooth $u_0(x)$, discontinuous solutions can develop after a finite time for this problem. Therefore, one has to seek solution to (2.2) in the weak form. To be more precise, let us recall that a bounded and measurable function $u(x,t)$, is a weak solution of (2.2) if the following equation is fulfilled

$$\iint_\Omega \Big(u\varphi_t + F(\gamma(x), u)\varphi_x \Big) dxdt + \int_{\mathbb{R}} u_0(x)\varphi(x,0)dx = 0,$$

for all test functions $\varphi \in C_0^\infty(\bar{\Omega})$. One can easily check that u is a weak solution of (2.2), if and only if, it satisfies in (1.1a)-(1.1b) in the weak sense. To ensure that u is conserved through a shock at the interface $x = 0$, any weak solution of (2.2) will satisfy the Rankine-Hugoniot condition for a zero-speed discontinuity, i.e., the flux coupling needs to be fulfilled for almost all $t > 0$

$$f_L(u(0^-, t)) = f_R(u(0^+, t)). \tag{2.3}$$

The existence of the (strong) traces $u(0^\pm, t)$ of the solution u from either sides at $x = 0$ can be concluded for instance from the results in [26].

In addition, a weak solution is not in general unique even in the case where the flux is smooth. Thus, an additional constraint is needed to choose the physically meaningful solution. This constraint is called an admissibility criterion or an entropy condition.

At $x \neq 0$, we need to specify a Kružkov-type entropy condition [27] which is derived from a regularization of the conservation laws. To proceed, we define the concept of an entropy pair. Functions $\{(\eta_\alpha, q_\alpha)\}_{\alpha=L,R}$ are called an entropy pair for (2.2), if and only if η_α is convex and $\eta'_\alpha(u)f'_\alpha(u) = q'_\alpha(u)$ for $\alpha = L, R$. Thus we have [28]:

Definition 2.1 (Interior entropy condition)**.** *A weak solution u of* (2.2) *satisfying* (2.3) *is said to be an interior entropy solution if the following entropy inequalities hold in the sense of*

distribution

$$\begin{aligned} \eta_R(u)\varphi_t + q_R(u)\varphi_x \le 0, \quad & \textit{in } x > 0, t > 0 \\ \eta_L(u)\varphi_t + q_L(u)\varphi_x \le 0, \quad & \textit{in } x < 0, t > 0 \end{aligned} \tag{2.4}$$

for every test function $\varphi \in C_0^\infty(\Omega)$ *with* $\varphi \ge 0$ *and for all entropy pairs* $(\eta_\alpha, q_\alpha), \alpha = L, R$.

Note that in the scalar case, every convex function η_α leads to an entropy pair by putting

$$q_\alpha(u) := \int^u \eta'_\alpha(\xi) f'_\alpha(\xi) d\xi, \quad \alpha = L, R. \tag{2.5}$$

It is well-known that for the problem (2.2) in which the flux function has a spatial discontinuity at the interface, the interior entropy conditions (2.3) itself is not enough to ensure the uniqueness and a new additional jump condition is needed to select a unique solution at $x = 0$. Several existence and uniqueness results for the entropy solutions of (2.2) have been derived both from mathematical and physical considerations in a series of papers; see [8] for a list of relevant references.

Following [13], in this work we assume that our flux function (2.2) satisfies a so-called "crossing condition". This restriction states that for any states u and v we must have

$$f_R(u) - f_L(u) < 0 < f_R(v) - f_L(v) \quad \Longrightarrow \quad u < v. \tag{2.6}$$

Geometrically, the crossing condition requires that either the graphs of f_L and f_R do not cross, or if they do, the graph of f_L lies above the graph of f_R to the left of any crossing point.

2.1. **Basic notations.** For solving numerically problem (2.2) provided with a suitable continuity constraint at the interface $x = 0$, we first introduce a uniform mesh of the spatial domain. We triangulate the spatial domain $\mathbb{R}$ with the partition $\mathcal{T}_h = \{K_j\}_{j\in\mathbb{Z}}$, where

$$K_j = \left[x_{j-\frac{1}{2}}, x_{j+\frac{1}{2}}\right], \quad j \in \mathbb{Z},$$

and for more convenience we set

$$x_{-\frac{1}{2}} = x_{\frac{1}{2}} := 0.$$

We will also set the midpoints as well as the width of the intervals as

$$x_j = \frac{1}{2}(x_{j-\frac{1}{2}} + x_{j+\frac{1}{2}}), \quad h_j = x_{j+\frac{1}{2}} - x_{j-\frac{1}{2}}; \quad h = \max_{1\le j\le N} h_j.$$

We assume that the mesh is quasi-uniform in the sense that there is a constant c independent of h such that $h_j \ge ch$ for all $j \in \mathbb{Z}$. To the mesh $\mathcal{T}_h$, we associate the finite element space $\mathcal{V}_h^k$, which is defined as piecewise polynomials space

$$\mathcal{V}_h^k := \left\{v \ : \ v|_K \in \mathbb{P}_k(K),\ K \in \mathcal{T}_h\right\},$$

where, $\mathbb{P}_k(K)$ denotes the set of polynomials of degree less than or equal to k on the cell $K \in \mathcal{T}_h$. Note that we may assume that the functions $v(x,t) \in \mathcal{V}_h^k$ are vanishing for sufficiently large $|x|$.

We shall use the following notation: Given a domain Q, we denote by $(.,.)_Q$ the usual $L_2(Q)$ scalar product, $\|.\| = \|.\|_{L_2(Q)}$ the corresponding L_2-norm, and for a positive integer

s, $H^s(Q)$ will denote the usual Sobolev space of functions with square integrable derivative of order less than or equal s and with the norm $\|.\|_{s,Q}$. Furthermore, for piecewise polynomial functions defined on the triangulation $\mathcal{T}_h$, we use the notation

$$\big(\cdot,\cdot\big)_Q = \sum_{K\in\mathcal{T}_h} (.,.)_K, \quad Q = \bigcup_{K\in\mathcal{T}_h} K,$$

i.e., we just sum the integrals over each element $K \in \mathcal{T}_h$. We also write for $t > 0$

$$\big(v,w\big)_j = \int_{K_j} v(x,t)w(x,t)dx, \quad \|v\|_j^2 = \big(v,v\big)_j,$$
$$v(x^{\pm}_{j\pm\frac{1}{2}}) = v(x^{\pm}_{j\pm\frac{1}{2}},t) = \lim_{s\longrightarrow 0^{\pm}} v(x_{j\pm\frac{1}{2}}+s,t).$$

2.2. **Projections.** For $k \geq 1$, we will consider two special Gauß-Radau projection operators, $\mathcal{P}_h^{\pm}$, which are defined as follows: For any smooth function w, the restriction of $\mathcal{P}_h^- w$ to K_j is defined as the unique element of $\mathbb{P}_k(K_j)$ satisfying

$$\big(\mathcal{P}_h^- w - w, v\big)_j = 0, \quad \forall v \in \mathbb{P}_{k-1}(K_j), \text{ and } \quad \mathcal{P}_h^- w(x^-_{j+\frac{1}{2}}) = w(x_{j+\frac{1}{2}}). \tag{2.7a}$$

Similarly, the projection $\mathcal{P}_h^+$ is defined as follows:

$$\big(\mathcal{P}_h^+ w - w, v\big)_j = 0, \quad \forall v \in \mathbb{P}_{k-1}(K_j), \text{ and } \quad \mathcal{P}_h^+ w(x^+_{j-\frac{1}{2}}) = w(x_{j-\frac{1}{2}}), \tag{2.7b}$$

where k is the degree of the DG solution. Notice that these two special projections are used in the error estimates of the DG methods to derive optimal L_2-error bounds in the literature, e.g., in [29]. Moreover, we consider the following projection $\mathcal{P}_h$ defined as

$$\big(\mathcal{P}_h w - w, v\big)_j = 0, \quad \forall v \in \mathbb{P}_k(K_j). \tag{2.7c}$$

From standard approximation theory [35] we have for $\pi_h = \mathcal{P}_h^-$ or $\pi_h = \mathcal{P}_h^+$ that

$$\|\pi_h w - w\| \leq Ch^{k+1}\|w\|_{k+1,\Omega}, \tag{2.8}$$

where w is the smooth exact solution and C is a generic constant independent of h and w. Throughout this paper, the projection π_h is defined element-wise and selected at each time level t corresponding to the sign variation of $f'_\alpha(u)$ for $\alpha = L, R$. If $f'_\alpha(u) > 0$, we choose $\pi_h = \mathcal{P}_h^-$; otherwise, we take $\pi_h = \mathcal{P}_h^+$.

3. The DG Formulation

The DG for (2.2) is derived from the weak formulation on each $K_j \in \mathcal{T}_h$, for $j \in \mathbb{Z}$. Multiplying equations (2.2) by an arbitrary test function v, integrating over the element K_j, and exploiting integration by parts by which we can couple weak form on K_j with weak forms

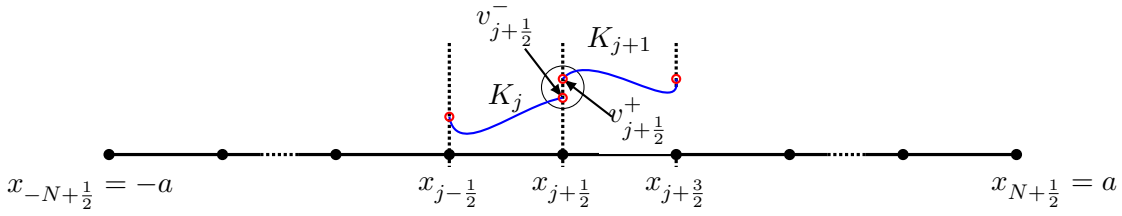

FIGURE 1. Partition of the space domain Ω_a into cells $K_j = [x_{j-\frac{1}{2}}, x_{j+\frac{1}{2}}]$ with cell width h_j and edges (interfaces) $x_{j\pm\frac{1}{2}}$. The open circles indicate the left and right limits of function v at interfaces.

on the other elements, we get

$$\big(u_t, v\big)_j - \big(f_R(u), v_x\big)_j + f_R(u)v\big|_{\partial K_j} = 0, \quad j \geq 1, \tag{3.1a}$$

$$\big(u_t, v\big)_j - \big(f_L(u), v_x\big)_j + f_L(u)v\big|_{\partial K_j} = 0, \quad j \leq -1, \tag{3.1b}$$

$$\big(u(x,0), v\big)_j = \big(u_0(x), v\big)_j, \quad j \in \mathbb{Z}. \tag{3.1c}$$

We replace the exact solution u by its possibly discontinuous approximation $u_h \in \mathcal{V}_h^k$. Since u_h is a discontinuous piecewise polynomial of degree k over the triangulation $\mathcal{T}_h$, it is not defined exactly on ∂K_j. There are many possible choices for these variables at the inter-element boundaries. The idea is to replace the flux functions $f_R(u)$ and $f_L(u)$ at the boundaries ∂K_j with the so-called "numerical fluxes" $\mathcal{F}_R(u)$ and $\mathcal{F}_L(u)$, which are single-valued functions defined at the cell interfaces and in general depending on the numerical solution u_h from both side of interfaces.

We can now formulate the discrete version of the weak forms (3.1a)-(3.1c) which are obtained by restricting the trial and test functions to finite dimensional subspace $\mathcal{V}_h^k$ and by exploiting the numerical fluxes $\mathcal{F}_R(u), \mathcal{F}_L(u)$ at the interfaces. Thus the semi-discrete DG for solving (2.2) is defined as follows: Find the unique function $u_h = u_h(t) \in \mathcal{V}_h^k$ such that for all test functions $v_h \in \mathcal{V}_h^k$ and for all $j \in \mathbb{Z}$ we have

$$\big(u_{h,t}, v_h\big)_j - \big(f_R(u_h), v_{h,x}\big)_j + \mathcal{F}_R^{j+\frac{1}{2}} v_h(x^-_{j+\frac{1}{2}}) - \mathcal{F}_R^{j-\frac{1}{2}} v_h(x^+_{j-\frac{1}{2}}) = 0, \ j \geq 1, \tag{3.2a}$$

$$\big(u_{h,t}, v_h\big)_j - \big(f_L(u_h), v_{h,x}\big)_j + \mathcal{F}_L^{j+\frac{1}{2}} v_h(x^-_{j+\frac{1}{2}}) - \mathcal{F}_L^{j-\frac{1}{2}} v_h(x^+_{j-\frac{1}{2}}) = 0, \ j \leq -1, \tag{3.2b}$$

$$\big(u_h(x,0), v_h\big)_j = \big(u_0(x), v_h\big)_j, \quad j \in \mathbb{Z}, \tag{3.2c}$$

where we have used the following notations for $\alpha = R, L$,

$$\mathcal{F}_\alpha^{j+\frac{1}{2}} = \mathcal{F}_\alpha(u_h(x^-_{j+\frac{1}{2}}, t), u_h(x^+_{j+\frac{1}{2}}, t)), \quad \mathcal{F}_\alpha^{j-\frac{1}{2}} = \mathcal{F}_\alpha(u_h(x^-_{j-\frac{1}{2}}, t), u_h(x^+_{j-\frac{1}{2}}, t)).$$

Note, in (3.2a)-(3.2b) for setting $v \equiv 1$, or equivalently, utilizing the piecewise constant $(k = 0)$, the considered DG method is just the classical finite volume methods. In Fig. 1, an illustration of the possible jumps in $v \in \mathcal{V}_h^k$ at element boundaries is presented.

Remark 3.1. *Observe that the coupling of the discrete DG schemes* (3.2a) *and* (3.2b) *is performed through the evaluation of two numerical fluxes* $\mathcal{F}_R^{+\frac{1}{2}} = \mathcal{F}_R(u_h(x_{\frac{1}{2}}^-, t), u_h(x_{\frac{1}{2}}^+, t))$ *and* $\mathcal{F}_L^{-\frac{1}{2}} = \mathcal{F}_L(u_h(x_{-\frac{1}{2}}^-, t), u_h(x_{-\frac{1}{2}}^+, t))$ *which need to utilize the values* $u_h(x_{\pm\frac{1}{2}}, t)$ *as the approximate solutions at points* $x_{\pm\frac{1}{2}} = 0^{\pm}$ *located on the right and left of the interface* $x = 0$.

Remark 3.2. *Instead of equation* (3.2c)*, usually the initial condition* $u_h(x, 0)$ *is taken as the* L_2*-projection of the analytical initial condition* $u_0(x)$ *onto the space of polynomials of degree* k*. Thus, with the projection defined in* (2.7c)*, we set* $u_h^0(x, 0) := \mathcal{P}_h u_0(x)$.

Here, for $\alpha = R, L$, the numerical flux $\mathcal{F}_\alpha$ is a monotone flux, i.e. $\mathcal{F}_\alpha$ is non-decreasing in the first argument and non-increasing in the second, symbolically $\mathcal{F}_\alpha(\uparrow, \downarrow)$. Also $\mathcal{F}_\alpha$ is Lipschitz continuous in both arguments, and is consistent with flux, i.e. $\mathcal{F}_\alpha(u, u) = f_\alpha(u)$. We will mainly use the simple upwind flux.

Since the functions in $\mathcal{V}_h^k$ are allowed to have discontinuities across element interfaces, one can exploit different local basis for finite element approximation. Let us choose a basis in the space $\mathbb{P}_k(K_j)$ formed by functions $\phi_0^j, \phi_1^j, \ldots, \phi_k^j$. Thus the numerical approximation $u_h(x, t)$ of $u(x, t)$ in every cell K_j can be expressed as

$$u_h(x, t) = \sum_{m=0}^{k} u_m^j(t)\phi_m^j(x), \quad x \in K_j, \quad j \in \mathbb{Z}, \tag{3.3}$$

where, $u_m^j(t), m = 0, \ldots, k$ are the moments or degrees of freedom with respect to time. Now, by taking $v_h = \phi_n^j(x), n = 0, 1, \ldots, k$ and putting that into (3.2a)-(3.2c) our scheme reads: Find $u_m^j,\ m = 0, \ldots, k$ such that

$$\begin{aligned}
&\Big(\sum_{m=0}^{k} \frac{d}{dt} u_m^j(t)\phi_m^j(x), \phi_n^j(x) \Big)_j - \Big(f_R\Big(\sum_{m=0}^{k} u_m^j(t)\phi_m^j(x) \Big), \frac{d}{dx}\phi_n^j(x) \Big)_j \\
&+ \mathcal{F}_R^{j+\frac{1}{2}} \Big(\sum_{m=0}^{k} u_m^j(t)\phi_m^j(x_{j+\frac{1}{2}}^-), \sum_{m=0}^{k} u_m^{j+1}(t)\phi_m^{j+1}(x_{j+\frac{1}{2}}^+) \Big) \phi_n^j(x_{j+\frac{1}{2}}^-) \qquad (3.4a) \\
&- \mathcal{F}_R^{j-\frac{1}{2}} \Big(\sum_{m=0}^{k} u_m^{j-1}(t)\phi_m^{j-1}(x_{j-\frac{1}{2}}^-), \sum_{m=0}^{k} u_m^j(t)\phi_m^j(x_{j-\frac{1}{2}}^+) \Big) \phi_n^j(x_{j-\frac{1}{2}}^+) = 0,
\end{aligned}$$

for all $j \geq 1$, and

$$\begin{aligned}
&\Big(\sum_{m=0}^{k} \frac{d}{dt} u_m^j(t)\phi_m^j(x), \phi_n^j(x)\Big)_j - \Big(f_L\Big(\sum_{m=0}^{k} u_m^j(t)\phi_m^j(x)\Big), \frac{d}{dx}\phi_n^j(x)\Big)_j \\
&+ \mathcal{F}_L^{j+\frac{1}{2}}\Big(\sum_{m=0}^{k} u_m^j(t)\phi_m^j(x_{j+\frac{1}{2}}^-), \sum_{m=0}^{k} u_m^{j+1}(t)\phi_m^{j+1}(x_{j+\frac{1}{2}}^+)\Big)\phi_n^j(x_{j+\frac{1}{2}}^-) \qquad (3.4b)\\
&- \mathcal{F}_L^{j-\frac{1}{2}}\Big(\sum_{m=0}^{k} u_m^{j-1}(t)\phi_m^{j-1}(x_{j-\frac{1}{2}}^-), \sum_{m=0}^{k} u_m^j(t)\phi_m^j(x_{j-\frac{1}{2}}^+)\Big)\phi_n^j(x_{j-\frac{1}{2}}^+) = 0,
\end{aligned}$$

for all $j \leq -1$, and

$$\sum_{m=0}^{k} u_m^j(0)\big(\phi_m^j(x), \phi_n^j(x)\big)_j = \big(u_0(x), \phi_n^j(x)\big)_j, \qquad (3.4c)$$

for all $j \in \mathbb{Z}$. Now by choosing a suitable numerical flux and using a special orthogonal basis functions to be specified below, our semi-discrete scheme will be transformed to a system of ordinary differential equation.

3.1. **The numerical flux coupling.** The choice of numerical flux determining stability as well as accuracy of the method and also affects e.g. the symmetry of the stiffness matrix. Therefore, we need to choose the numerical flux $\mathcal{F}_\alpha$ for $\alpha = L, R$ appropriately. In this work our numerical flux is taken as upwind flux. We recall that a numerical flux $\mathcal{F}(u)$ (associated with flux function $f(u)$) is called *upwind* if it satisfies

$$\mathcal{F}(u) = \begin{cases} f(u^-), & f'(u) \geq 0, \quad \forall u \in [\min(u^-, u^+), \max(u^-, u^+)], \\ f(u^+), & f'(u) < 0, \quad \forall u \in [\min(u^-, u^+), \max(u^-, u^+)]. \end{cases}$$

The best-known examples of upwind numerical fluxes are the Godunov flux, the Engquist-Osher flux, the Lax-Friedrichs flux, and the Roe flux with an entropy fix. For more details, see for example [30]. As mentioned earlier, in order to complete the definition of the scheme we need to select $\mathcal{F}_\alpha$ on the boundaries of K_j. We choose the upwind flux in (3.4a)-(3.4b) depending on whether the corresponding characteristic speed on each K_j is positive or negative, e.g., $f'_\alpha(u_h(x_{j\pm\frac{1}{2}}^{\pm}, \cdot)) \gtrless 0$. For $\alpha = L, R$, if $f'_\alpha(u) > 0$, we take simply

$$\mathcal{F}_\alpha^{j\pm\frac{1}{2}} = f_\alpha(u_h(x_{j\pm\frac{1}{2}}^-)), \quad j \in \mathbb{Z},\ j \neq -1 \text{ or } 1, \qquad (3.5a)$$

and if $f'_\alpha(u) < 0$, we set

$$\mathcal{F}_\alpha^{j\pm\frac{1}{2}} = f_\alpha(u_h(x_{j\pm\frac{1}{2}}^+)), \quad j \in \mathbb{Z}, j \neq -1 \text{ or } 1, \qquad (3.5b)$$

In order to define the numerical coupling procedure, at the coupling interface labeled by index $j=-1$, or $j=1$ or both $j=\pm 1$ we need to determine the numerical fluxes $\mathcal{F}_{\alpha}^{\pm\frac{1}{2}}, \alpha = L, R$ precisely. For this purpose, we distinguish between the following three cases.

i) $f'_L(u) > 0$ and $f'_R(u) > 0$: In this cases it is sufficient to take

$$\mathcal{F}_R^{+\frac{1}{2}} := f_L(u_h(x^-_{-\frac{1}{2}})). \tag{3.6a}$$

ii) $f'_L(u) < 0$ and $f'_R(u) < 0$: As opposed to the first case, we set

$$\mathcal{F}_L^{-\frac{1}{2}} := f_R(u_h(x^+_{\frac{1}{2}})). \tag{3.6b}$$

iii) $f'_L(u) > 0$ and $f'_R(u) < 0$: As the simplest case we do not need any coupling condition at the interface and the numerical fluxes defined in (3.5a) and (3.5b) work.

Remark 3.3. *We emphasize that if $f'_L(u) < 0$ and $f'_R(u) > 0$, the solution $u(x,t)$ is not defined in the fan $f'_L(u) < \frac{x}{t} < f'_R(u)$, and one can in fact construct an infinite number of solutions of the problem by specifying $u(0,t)$ at the interface. In view of two former cases, selecting the numerical fluxes as* (3.6a) *and* (3.6b) *may not work in general. Depending on the prescribed coupling condition $u(0,t)$, the numerical fluxes can be taken for $\alpha = L, R$ as*

$$\mathcal{F}_R^{+\frac{1}{2}} := f_L(u(0^-,t)), \quad \textit{and} \quad \mathcal{F}_L^{-\frac{1}{2}} := f_R(u(0^+,t)), \quad t>0.$$

4. Stability Estimates for the DG

In order to prove the basic stability estimates for the DG scheme (3.2), we introduce the following bilinear form for $\alpha = L, R$,

$$\mathbb{B}_{\alpha}^{j}(u_h, v_h) := \int_{K_j} u_{h,t} v_h dx - \int_{K_j} f_{\alpha}(u_h) v_{h,x} dx + \mathcal{F}_{\alpha}^{j+\frac{1}{2}} v_h(x^-_{j+\frac{1}{2}}) - \mathcal{F}_{\alpha}^{j-\frac{1}{2}} v_h(x^+_{j-\frac{1}{2}}).$$

Now, our DG scheme reads: find the function $u_h \in \mathcal{V}_h^k$ such that

$$\mathbb{B}_L^j(u_h, v_h) = 0, \quad \forall v_h \in \mathcal{V}_h^k, \quad j \le -1, \tag{4.1a}$$

$$\mathbb{B}_R^j(u_h, v_h) = 0, \quad \forall v_h \in \mathcal{V}_h^k, \quad j \ge 1. \tag{4.1b}$$

In what follows, we will prove that the scheme (4.1) satisfies the (interior) cell entropy inequality (2.4) for the square entropy

$$\mathbb{U}(u) := \eta_{\alpha}(u) = \frac{u^2}{2}, \tag{4.2}$$

for $\alpha = L, R$. In the following, we assume that $f'_{\alpha}(u(x,t)) > 0, \forall (x,t) \in \Omega$, for $\alpha = L, R$. We note that the other case $f'_{\alpha}(u(x,t)) \gtrless 0$ can be handled in a very similar way and hence we omit it. Now, we will state an analogue entropy inequality for the approximation scheme (4.1), a similar proof can be found in [31].

Lemma 4.1 (Interior cell entropy inequality)**.** *The solution u_h to the semi-discrete DG scheme* (4.1) *satisfies the following cell entropy inequality for $\alpha = L, R$*

$$\frac{d}{dt}\int_{K_j} \mathbb{U}(u_h)dx + \widehat{\mathcal{F}}_\alpha^{j+\frac{1}{2}} - \widehat{\mathcal{F}}_\alpha^{j-\frac{1}{2}} \leq 0, \quad j \neq 1, \tag{4.3}$$

for the square entropy (4.2) *and for some consistent entropy flux*

$$\widehat{\mathcal{F}}_\alpha^{j\pm\frac{1}{2}} = \widehat{\mathcal{F}}_\alpha(u_h(x^-_{j\pm\frac{1}{2}}, t), u_h(x^+_{j\pm\frac{1}{2}}, t)),$$

satisfying $\widehat{\mathcal{F}}_\alpha(u,u) = q_\alpha(u)$.

Proof. We prove the result for $\alpha = R$, which corresponds to $j \geq 2$. The proof in the case $\alpha = L$ and $j \leq -1$ is similar. Let us define $g_\alpha(u) := \int^u f_\alpha(u)du, \alpha = L, R$. By taking $v_h = u_h$ in $\mathbb{B}_R^j$ we get

$$\begin{aligned}
\mathbb{B}_R^j(u_h, u_h) &= \int_{K_j} u_{h,t}u_h dx - \int_{K_j} f_R(u_h)u_{h,x}dx + \mathcal{F}_R^{j+\frac{1}{2}}u_h(x^-_{j+\frac{1}{2}}) - \mathcal{F}_R^{j-\frac{1}{2}}u_h(x^+_{j-\frac{1}{2}}) \\
&= \int_{K_j} \frac{1}{2}(u_h^2)_t dx - \int_{K_j} g(u_h)_x dx + \mathcal{F}_R^{j+\frac{1}{2}}u_h(x^-_{j+\frac{1}{2}}) - \mathcal{F}_R^{j-\frac{1}{2}}u_h(x^+_{j-\frac{1}{2}}) \\
&= \int_{K_j} \mathbb{U}(u_h)_t dx - g_R(u_h(x^-_{j+\frac{1}{2}})) + g_R(u_h(x^+_{j-\frac{1}{2}})) \\
&+ \mathcal{F}_R^{j+\frac{1}{2}}u_h(x^-_{j+\frac{1}{2}}) - \mathcal{F}_R^{j-\frac{1}{2}}u_h(x^+_{j-\frac{1}{2}}) \\
&= \frac{d}{dt}\int_{K_j} \mathbb{U}(u_h)dx + \widehat{\mathcal{F}}_R^{j+\frac{1}{2}} - \widehat{\mathcal{F}}_R^{j-\frac{1}{2}} + \Theta_R^{j-\frac{1}{2}} = 0,
\end{aligned} \tag{4.4}$$

where we have used

$$\begin{aligned}
\widehat{\mathcal{F}}_R^{j\pm\frac{1}{2}} &:= -g_R(u_h(x^-_{j\pm\frac{1}{2}})) + \mathcal{F}_R^{j\pm\frac{1}{2}}u_h(x^-_{j\pm\frac{1}{2}}), \\
\Theta_R^{j-\frac{1}{2}} &:= -g_R(u_h(x^-_{j-\frac{1}{2}})) + \mathcal{F}_R^{j-\frac{1}{2}}u_h(x^-_{j-\frac{1}{2}}) + g_R(u_h(x^+_{j-\frac{1}{2}})) - \mathcal{F}_R^{j-\frac{1}{2}}u_h(x^+_{j-\frac{1}{2}}).
\end{aligned}$$

It suffices to show that $\widehat{\mathcal{F}}_R$ is consistent and $\Theta_{j-\frac{1}{2}} \geq 0$. To prove consistency, first note that $\widehat{\mathcal{F}}_R(u,u) = -g_R(u) + f_R(u)u$. Next, by $q_R(u)$ according to (2.5) we have

$$q_R(u) = \int^u \mathbb{U}'(u)f_R'(u)du = \int^u u df_R(u)du = uf_R(u) - \int^u f_R(u)du = uf_R(u) - g_R(u),$$

which means that $\widehat{\mathcal{F}}_R(u,u) = q_R(u)$. To prove positivity of $\Theta^R_{j-\frac{1}{2}}$, by dropping the subscript we get

$$\begin{aligned}\Theta^R &= -g_R(u^-) + \mathcal{F}_R(u^-,u^+)u^- + g_R(u^+) - \mathcal{F}_R(u^-,u^+)u^+\\ &= g_R(u^+) - g_R(u^-) - \mathcal{F}_R(u^-,u^+)(u^+-u^-)\\ &= g'_R(\eta)(u^+-u^-) - \mathcal{F}_R(u^-,u^+)(u^+-u^-) = \Big(g'_R(\eta) - \mathcal{F}_R(u^-,u^+)\Big)(u^+-u^-)\\ &= \Big(\mathcal{F}_R(\eta,\eta) - \mathcal{F}_R(u^-,u^+)\Big)(u^+-u^-),\end{aligned}$$

where η is in between u^- and u^+. Now, the monotonicity of the flux function $\mathcal{F}_R$ completes our proof. □

Remark 4.2. *For $j = 1$, i.e., on the element K_1, an analogue inequality like* (4.3) *can be obtained. In this case we have*

$$\frac{d}{dt}\int_{K_1} \mathbb{U}(u_h)dx + \widehat{\mathcal{F}}^{\frac{3}{2}}_R - \widehat{\mathcal{F}}^{+\frac{1}{2}}_R \le 0, \tag{4.5}$$

where $\widehat{\mathcal{F}}^{\frac{3}{2}}_R$ is defined as in Lemma 4.1 and $\widehat{\mathcal{F}}^{+\frac{1}{2}}_R = \mathcal{F}^{+\frac{1}{2}}_R u_h(x^+_{\frac{1}{2}})$.

5. Convergent Analysis: Linear Case

In this section, we show the optimal convergent rate property of the DG solutions toward a particular projection of the exact solution when the upwind fluxes are used. To obtain optimal L_2-error estimates for the DG scheme (4.1), we assume that the exact solution of (2.2) is smooth. For simplicity we will give here the proof only for the linear version of (2.2), namely

$$f_\alpha(u) = a_\alpha u, \quad \alpha = L, R. \tag{5.1}$$

Without loss of generality we assume that $f'_\alpha = a_\alpha > 0$ for $\alpha = L, R$, for which the upwind flux (3.5a) is applied. For the linear flux (5.1), the projection π_h solely depends on the sign of a_α, i.e., $\pi_h = \mathcal{P}^-_h$ if $a_\alpha > 0$.

In the following, we will consider various measurements of errors. Let us denote $e = u - u_h$ to be the error between the exact solution and the numerical solution, $\eta = u - \mathcal{P}^-_h u$, the projection error, and $\xi = u_h - \mathcal{P}^-_h u$ the error between the numerical solution and the projection of the exact solution. Furthermore, it is easy to verify that the exact solution of (2.2) also for all $v_h \in \mathcal{V}^k_h$ and for all j satisfies

$$\mathbb{B}^j_\alpha(u, v_h) = 0, \quad \alpha = L, R. \tag{5.2}$$

Now subtracting (4.1) from (5.2) we get the following *Galerkin orthogonality* property:

$$\mathbb{B}^j_\alpha(u - u_h, v_h) = \mathbb{B}^j_\alpha(e, v_h) = 0, \quad \alpha = L, R, \tag{5.3}$$

for all $v_h \in \mathcal{V}^k_h$ and for all j, which is very useful in our error estimates below [34].

Theorem 5.1. *Let u be the smooth exact solution of* (2.2) *with $f_\alpha(u) = a_\alpha u, \alpha = L, R$, and let u_h be the numerical solution of the DG scheme* (4.1) *with the upwind flux* (3.5)*, then*

$$\|u - u_h\| \leq Ch^{k+1}\|u\|_{k+1,\mathbb{R}}, \tag{5.4}$$

where C is a constant independent of h and u.

Proof. By means of Galerkin orthogonality relation (5.3) we have for $\alpha = L, R$ that

$$\mathbb{B}^j_\alpha(e, v_h) = \mathbb{B}^j_\alpha(u - \mathcal{P}^-_h u + \mathcal{P}^-_h u - u_h, v_h) = \mathbb{B}^j_\alpha(\eta - \xi, v_h) = 0, \quad v_h \in \mathcal{V}^k_h.$$

In the last equality we set $v_h = \xi = u_h - \mathcal{P}^-_h u \in \mathcal{V}^k_h$ to obtain

$$\mathbb{B}^j_\alpha(\eta - \xi, \xi) = 0,$$

from which one can immediately conclude that

$$\mathbb{B}^j_\alpha(\xi, \xi) = \mathbb{B}^j_\alpha(\eta, \xi). \tag{5.5}$$

The cell entropy inequality (4.4) for $\alpha = L, R$ gives

$$\mathbb{B}^j_L(\xi, \xi) = \frac{1}{2}\frac{d}{dt}\|\xi\|^2_j + \widehat{\mathcal{F}}^{j+\frac{1}{2}}_L - \widehat{\mathcal{F}}^{j-\frac{1}{2}}_L + \Theta^{j-\frac{1}{2}}_L, \quad j \leq -1, \tag{5.6a}$$

$$\mathbb{B}^j_R(\xi, \xi) = \frac{1}{2}\frac{d}{dt}\|\xi\|^2_j + \widehat{\mathcal{F}}^{j+\frac{1}{2}}_R - \widehat{\mathcal{F}}^{j-\frac{1}{2}}_R + \Theta^{j-\frac{1}{2}}_R, \quad j \geq 2, \tag{5.6b}$$

where $\Theta^{j-\frac{1}{2}}_\alpha \geq 0$ for $\alpha = L, R$. With an analogue argument as (4.5), one can show that

$$\mathbb{B}^1_R(\xi, \xi) = \frac{1}{2}\frac{d}{dt}\|\xi\|^2_1 + \widehat{\mathcal{F}}^{\frac{3}{2}}_R - \widehat{\mathcal{F}}^{+\frac{1}{2}}_R. \tag{5.6c}$$

For the right-hand side of (5.5), according to (4.1) and using (2.7a) we have

$$\mathbb{B}^j_\alpha(\eta, \xi) = \big(\eta_t, \xi\big)_j - \big(a_\alpha \eta, \xi_x\big)_j + (a_\alpha \eta(x^-_{j+\frac{1}{2}}))\xi(x^-_{j+\frac{1}{2}}) - (A^j_\alpha \eta(x^-_{j-\frac{1}{2}}))\xi(x^+_{j-\frac{1}{2}}), \quad \alpha = L, R.$$

Here the constant A^j_α is defined as

$$A^j_\alpha = \begin{cases} a_L, & \alpha = L, j \leq -1, \\ a_L, & \alpha = R, j = 1, \\ a_R, & \alpha = R, j \geq 2. \end{cases}$$

Now, using the fact that $\xi_x \in \mathbb{P}_{k-1}(K_j)$ and by (2.7a) we find that

$$\big(\eta, \xi_x\big)_j = 0, \quad \text{and} \quad \eta^-_{j\pm\frac{1}{2}} = u(x_{j\pm\frac{1}{2}}) - \mathcal{P}^-_h u(x^-_{j\pm\frac{1}{2}}) = 0.$$

Applying the inequality $ab \leq \frac{1}{2}a^2 + \frac{1}{2}b^2$, we therefore obtain

$$\mathbb{B}^j_\alpha(\eta, \xi) = \big(\eta_t, \xi\big)_j \leq \frac{1}{2}\|\eta_t\|^2_j + \frac{1}{2}\|\xi\|^2_j. \tag{5.7}$$

By substituting (5.6a)-(5.6c) and (5.7) into (5.5) and summing up over $j \in \mathbb{Z}$ we get

$$\frac{d}{dt}\|\xi(t)\|^2 \leq \|\xi(t)\|^2 + \|\eta_t\|^2 \leq \|\xi(t)\|^2 + Ch^{2k+2}\|u\|^2_{k+1,\mathbb{R}}, \tag{5.8}$$

where in the last inequality we have used the approximation result (2.8)

$$\|\eta_t\| = \|u_t - (\mathcal{P}_h^- u)_t\| = \|u_t - \mathcal{P}_h^-(u_t)\| \leq Ch^{k+1}\|u\|_{k+1,\mathbb{R}}.$$

Integrating (5.8) from 0 to t and using the fact that the initial error satisfies

$$\|\xi(0)\| = \|u_h(\cdot,0) - \mathcal{P}_h^- u_h(\cdot,0)\| = \|u_0 - \mathcal{P}_h^- u_0\| = 0,$$

and employing the Gronwall's inequality we arrive at

$$\|\xi\| \leq ch^{k+1}\|u\|_{k+1,\mathbb{R}},$$

Combined with $\|e\| \leq \|\xi\| + \|\eta\|$ and the error estimate (2.8), we have finished the proof. □

Remark 5.2. *The a priori error estimates* (5.4) *for the DG scheme should be compared with the following estimate for the standard Galerkin method*

$$\|u - u_h\| \leq Ch^k\|u\|_{k+1,\Omega},$$

for the hyperbolic problems, which is obviously not-optimal, and for the shock-capturing methods, like the streamline diffusion method (cf. [25]*)*

$$\|u - u_h\| \leq Ch^{k+\frac{1}{2}}\|u\|_{k+1,\Omega},$$

for the hyperbolic problems, which is sub-optimal.

6. Practical Implementation

By putting $f_\alpha(u) = a_\alpha u$ for $\alpha = L, R$ in (1.1) we get the linear case of our model problem

$$\begin{cases} u_t + a_R u_x &= 0, & x \in (0,1), & t \in (0,T), \\ u_t + a_L u_x &= 0, & x \in (-1,0), & t \in (0,T), \\ u(x,0) &= u_0(x), & x \in (-1,1). \end{cases} \tag{6.1}$$

Note that in this case the crossing condition (2.6) will be automatically satisfied. Without loss of generality, we assume that

$$a_L > 0 \quad \text{and} \quad a_R > 0, \tag{6.2}$$

for which we utilize (3.5a) for the left and right fluxes, far away from the interface. For the two neighboring cells K_{-1} and K_1 surrounding the interface $x = 0$, we make use of numerical fluxes (3.5a) and (3.6a) respectively. The three remaining cases $a_L \gtrless 0$ and $a_R \gtrless 0$ can be treated analogously. Furthermore, we restrict ourselves to the computational domain $\Omega = (-1,1) \times (0,T)$, for which the corresponding spatial partition with $2N$ cells takes the form

$$-1 =: x_{-N-\frac{1}{2}} < \ldots < x_{-\frac{3}{2}} < x_{\pm\frac{1}{2}} = 0 < x_{\frac{3}{2}} < \ldots < x_{N+\frac{1}{2}} := 1.$$

In this part, our aim is to implement the DG scheme (3.4) for the model problem (6.1) efficiently and accurately. Our strategy is based on Legendre polynomials. As we shall see, this

will produce a diagonal mass matrix without a need to use lumping. Due to their orthogonality property on $[-1,1]$, we map every element K_j onto the reference element $[-1,1]$ by introducing a local coordinate $\xi \in [-1,1]$ such that

$$\xi(x) = \frac{2(x-x_j)}{h_j}.$$

Now, we choose $\phi_m^j(x) = P_m(\xi)$ in (3.3) for $j = 1,2,\ldots,N$, where P_m is the Legendre polynomial of degree m in ξ. With this transformation, the unknown values $u_m^j(t)$ in (3.3) can be interpreted as the Legendre coefficients of the expansion of $u_h(x,t)$. Recall that, the Legendre polynomials satisfy the following relations [33]

$$\int_{-1}^{1} P_m(\xi)P_n(\xi)d\xi = \frac{2\delta_{mn}}{2m+1}, \quad P_m(1) = 1, \quad P_m(\xi) = (-1)^m P_m(-\xi), \tag{6.3a}$$

$$(2m+1)P_m(\xi) = P'_{m+1}(\xi) - P'_{m-1}(\xi), \tag{6.3b}$$

for $m,n \geq 0$. Here, δ_{mn} is the Kronecker delta. The m'th degree Legendre polynomials $P_m(\xi)$ can be generated by the Rodriguez formula

$$P_m(\xi) = \frac{1}{2^m m!}\frac{d^m}{dx^m}(\xi^2-1)^m.$$

However, there is a more stable way to compute the Legendre polynomials at some point ξ by the following recursive relation

$$P_{m+1}(\xi) = \frac{2m+1}{m+1}\xi P_m(\xi) - \frac{m}{m+1}P_{m-1}(\xi), \quad P_0(\xi) = 1, \quad P_1(\xi) = \xi, \quad m = 1,2,\cdots.$$

Now, by the virtue of the Legendre properties (6.3a) and numerical upwinding fluxes (3.5a)-(3.5b), the DG scheme (3.4a)-(3.4b) can be written for $n = 0,1,\ldots,k$ as

$$\sum_{m=0}^{k}\frac{d}{dt}u_m^{j,R}M_{mn} = a_R\Big\{\sum_{m=0}^{k}\Big(D_{mn}-1\Big)u_m^{j,R} + (-1)^n\sum_{m=0}^{k}u_m^{j-1,R}\Big\}, \quad j = 2,\ldots,N, \tag{6.4a}$$

$$\sum_{m=0}^{k}\frac{d}{dt}u_m^{j,L}M_{mn} = a_L\Big\{\sum_{m=0}^{k}\Big(D_{mn}+(-1)^{m+n}\Big)u_m^{j,L} - \sum_{m=0}^{k}(-1)^m u_m^{j+1,L}\Big\}, j = -N,\ldots,-1, \tag{6.4b}$$

for all $j \neq 1$. Note that the approximated solutions $u_m^{1,R}$, $m = 0,1,\ldots,k$ on the right-hand side of the interface, i.e. in $K_1 = [x_{\frac{1}{2}}, x_{\frac{3}{2}}]$ are obtained by using the numerical flux coupling (3.6a), since the advection velocity is positive there due to our assumption (6.2). In view of (3.6a), the numerical solutions $u_m^{1,R}$, $m = 0,1,\ldots,k$ can be written for $n = 0,1,\ldots,k$ as

$$\sum_{m=0}^{k}\frac{d}{dt}u_m^{1,R}M_{mn} = a_R\Big\{\sum_{m=0}^{k}\Big(D_{mn}-1\Big)u_m^{1,R}\Big\} + a_L(-1)^n\sum_{m=0}^{k}u_m^{-1,L}. \tag{6.4c}$$

The components M_{mn} and D_{mn} as the entries of the mass matrix $\boldsymbol{M}_j$ and stiffness matrix $\boldsymbol{D}$ are defined as follows

$$M_{mn} = \frac{dx}{d\xi}\int_{-1}^{1} P_m(\xi)P_n(\xi)d\xi = \begin{cases} \frac{h_j}{2}\frac{2}{2n+1}, & n = m, \\ 0, & n \neq m, \end{cases} \qquad D_{mn} = \frac{dx}{d\xi}\int_{-1}^{1} P_m(\xi)\frac{d}{dx}P_n(\xi)d\xi.$$

To evaluate D_{mn}, we first perform a simple change of variable to obtain

$$D_{mn} = \int_{-1}^{1} P_m(\xi)\frac{d}{d\xi}P_n(\xi)d\xi.$$

Then, from the Legendre property (6.3b) we derive recursively

$$P'_{n+1} = (2n+1)P_n + (2(n-1)+1)P_{n-2} + (2(n-4)+1)P_{n-4} + \dots. \tag{6.5}$$

Now, applying the orthogonality property of the Legendre polynomials (6.3a) to equation (6.5), simplify the integral in D_{mn} as follows

$$D_{mn} = \begin{cases} 2, & n > m \text{ and } n+m \text{ is even}, \\ 0, & \text{otherwise}. \end{cases}$$

Note that all the (local) mass matrices $\boldsymbol{M}_j$, for $j = -N, \dots, N$ and $\boldsymbol{D}$ are of dimension $(k+1)\times(k+1)$, moreover, the mass matrices $\boldsymbol{M}_j$ are also diagonal due to the orthogonality of Legendre polynomials.

By introducing $\boldsymbol{U}_j^{\alpha} = [u_0^{j,\alpha}, u_1^{j,\alpha}, \dots, u_k^{j,\alpha}]^T$, the above equations (6.4a)-(6.4c) can be written in a matrix form. Here $\alpha = L, R$ denote the solution coefficients on the left and right of computational domain. Thus, the whole scheme reads

$$\boldsymbol{M}_j\frac{d}{dt}\boldsymbol{U}_j^R = a_R\Big(\boldsymbol{D}+\boldsymbol{E}\Big)\boldsymbol{U}_j^R - a_R\boldsymbol{F}\boldsymbol{U}_{j+1}^R, \quad j = 2, \dots, N, \tag{6.6a}$$

$$\boldsymbol{M}_j\frac{d}{dt}\boldsymbol{U}_j^L = a_L\Big(\boldsymbol{D}-\boldsymbol{G}\Big)\boldsymbol{U}_j^L + a_L\boldsymbol{F}^T\boldsymbol{U}_{j-1}^L, \quad j = -N, \dots, -1, \tag{6.6b}$$

$$\boldsymbol{M}_j\frac{d}{dt}\boldsymbol{U}_j^R = a_R\Big(\boldsymbol{D}+\boldsymbol{E}\Big)\boldsymbol{U}_j^R - a_L\boldsymbol{F}\boldsymbol{U}_{-j}^L, \quad j = 1, \tag{6.6c}$$

where

$$\boldsymbol{E}_{mn} = (-1)^{m+n}, \quad \boldsymbol{F}_{mn} = (-1)^m, \quad \boldsymbol{G}_{mn} = 1.$$

Considering the initial condition (3.4b), using the fact that each local mass matrix $\boldsymbol{M}_j$ is invertible, we can express the systems (6.6a)-(6.6c) in the compact form

$$\begin{cases} \boldsymbol{U}_t = L(\boldsymbol{U}), & t \in [0,T], \\ \boldsymbol{U}(0) = \boldsymbol{U}_0, \end{cases}$$

where $\boldsymbol{U} = [\boldsymbol{U}^L \quad \boldsymbol{U}^R]^T$ with $\boldsymbol{U}^{\alpha} = [\boldsymbol{U}_1^{\alpha}, \boldsymbol{U}_2^{\alpha}, \dots, \boldsymbol{U}_N^{\alpha}]^T$ for $\alpha = L, R$.

So far, we have only described the spatial discretization and have left the time variable t continuous. To preserve stability of the scheme, time discretization is performed by the TVD

high order of the Runge-Kutta methods developed in [20]. The third-order of the TVD-Runge-Kutta method used in this paper is as follows:

$$\begin{aligned} \boldsymbol{U}^{(1)} &= \boldsymbol{U}^n + \Delta t L(\boldsymbol{U}^n), \\ \boldsymbol{U}^{(2)} &= \frac{3}{4}\boldsymbol{U}^n + \frac{1}{4}\boldsymbol{U}^{(1)} + \frac{1}{4}\Delta t L(\boldsymbol{U}^{(1)}), \\ \boldsymbol{U}^{n+1} &= \frac{1}{3}\boldsymbol{U}^n + \frac{2}{3}\boldsymbol{U}^{(2)} + \frac{2}{3}\Delta t L(\boldsymbol{U}^{(2)}). \end{aligned} \tag{6.7}$$

The size of a stable time-step Δt depends not only on the order of a discontinuous Galerkin scheme but also the stability region of the chosen time integration scheme. For a single advection equation, there is a conjecture which says that for RKDG discretization using polynomials of degree k and a $k+1$ stage RK method, we can take CFL (Courant-Fredriches-Lewy) stability limit as [22]

$$|a|\frac{\Delta t}{\Delta x} \leq \frac{1}{2k+1},$$

where a is the advection speed and Δx is the element width (here $\Delta x = h$). This fact is proved for $k = 1$, however, no theoretical proof exists for larger $k \geq 1$. For the coupled advection problem (6.1), in the following experiments we always assume that $\max\{|a_L|, |a_R|\} < 1$. Thus, to fulfil the CFL condition we choose the least time-step as $\Delta t = \min_j \frac{h_j}{2k+1}$ while the three stages temporal discretization scheme (6.7) is used.

7. NUMERICAL RESULTS

To show the performance of the previously described method, we consider our model problem (6.1) with different advection speeds $a_\alpha \gtrless 0$ for $\alpha = L, R$, and various initial conditions. In the computation below, our domain is $[-1, 1]$, compactly supported boundary conditions are imposed, and our numerical initial condition is taken by the L_2-projection of the initial condition.

We solve this problem using the DG method on uniform meshes with the mesh width h obtained by partitioning the domain $[-1, 1]$ into N subintervals with $N = 2^s, s = 4, 5, \cdots, 10$ and using the spaces $\mathbb{P}_k$ with $k = 0, 1, \cdots, 6$. The time interval $[0, T]$ is divided into $nt = \lceil \frac{T}{\Delta t} \rceil$ small time-step $\Delta t = \frac{h}{2k+1}$, where $h = 2/N$. Here, the final time is taken as $T = 0.5$.

We also calculate the L_*-norm error, namely $\|e_h\|_* = \|u_h - u_{exact}\|_*$, where $*$ stands for L_1, L_2 or L_∞ norm. The relative error norms of numerical solutions u_h are defined by

$$E_* \equiv E_{*,h} = \frac{\|e_h\|_*}{\|u_{exact}\|_*}. \tag{7.1}$$

Moreover, we compute the order of convergence rate of the RKDG scheme through defining the convergence ratio $r = \frac{E_{*,h}}{E_{*,\frac{h}{2}}}$ and then calculating $\log_2(r)$. We remark that temporal discretization of all numerical examples is performed by the third-order accurate TVD Runge-Kutta method (6.7), with a sufficiently small time-step Δt so that the error in time is negligible compared to the spatial error, unless otherwise stated.

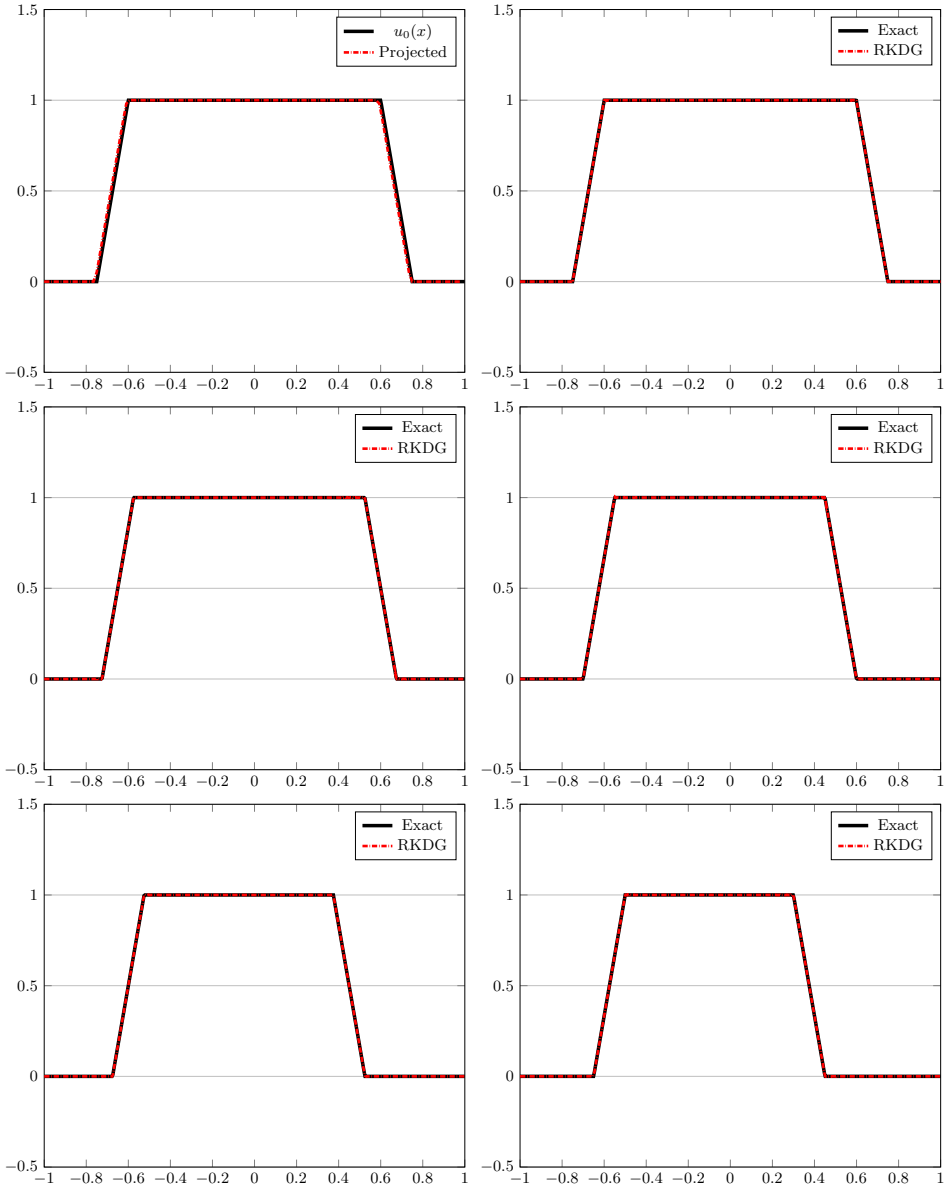

FIGURE 2. Numerical and exact solutions of Example 7.1 at time instants $t = 0, \Delta t$ (top), $t = 88\Delta t, 176\Delta t$ (middle), and $t = 264\Delta t, 352\Delta t$ (bottom). In all plots, $k = 5$, $N = 128$, and solid curves correspond to the exact solutions.

Example 7.1 ($a_L > 0$, $a_R < 0$). *We first consider the one-dimensional coupling of two advection equations* (6.1) *with wave speeds* $a_L = 0.2$ *and* $a_R = -0.6$ *and a piecewise continuous*

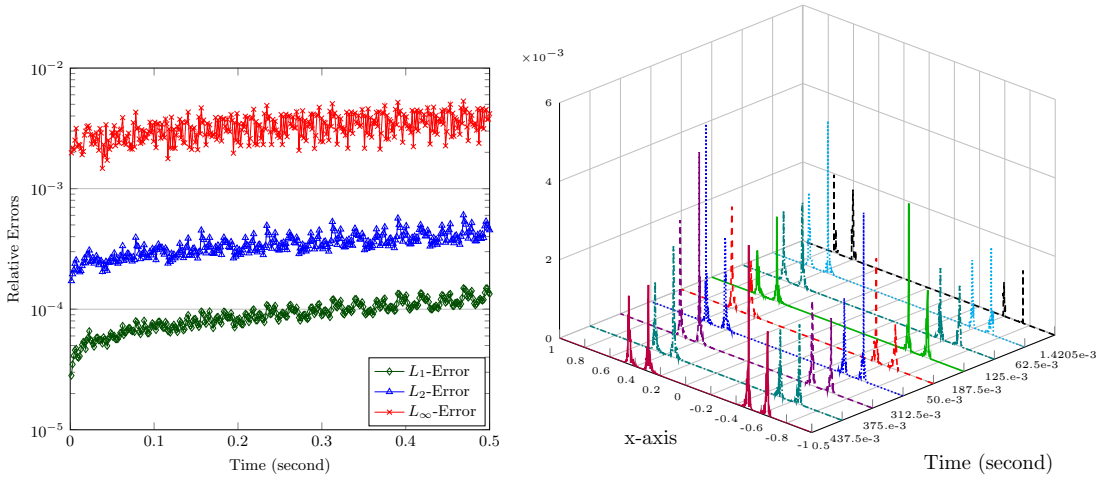

FIGURE 3. Relative L_2, L_1, and L_∞ errors for Example 7.1 versus time t (left). Absolute errors of Example 7.1 at different time instants $t = s\Delta t, s = 1, 44, 88, 132, 176, 220, 264, 352$ (right). In both cases, $k = 5$ and $N = 128$.

initial data $u_0(x)$ *is defined as*

$$u_0(x) = \begin{cases} 0, & |x| \geq 0.75, \\ \frac{x+0.75}{0.15}, & -0.75 < x \leq -0.60, \\ 1, & |x| \leq 0.60, \\ 1 - \frac{x-0.60}{0.15}, & 0.60 < x \leq 0.75. \end{cases}$$

In this case, the exact solution (6.1) *is given by*

$$u(x,t) = \begin{cases} u_0(x - a_L t), & x < 0, \\ u_0(x - a_R t), & x > 0. \end{cases}$$

First, for a fixed $N = 128$ and $k = 5$ we plot the numerical solutions as well as the exact solutions at different time instants $t = 0, \Delta t, 88\Delta t, 176\Delta t, 264\Delta t$, and $t = 352\Delta t$ in Fig. 2. At the time $t = 0$, the initial condition $u_0(x)$ and its (projected) approximation are plotted (see Fig. 2, top left). In all plots, the exact solutions are indicated by solid lines while the numerical counterpart are depicted by (red) dashed lines. It can be seen from Fig. 2 that the numerical solutions are very close to the exact ones. For this example, we also investigate the behavior of relative errors with respect to time in three different norms L_1, L_2, and L_∞ as shown in Fig. 3, left. In the latter Fig. 3, the absolute errors at different time instants $t = s\Delta t$, for $s = 1, 88, 176, 264, 352$ are additionally presented.

Example 7.2 ($a_L > 0$, $a_R > 0$). *As the second example to see the advantages of RKDG scheme, we consider the following example*

$$u_0(x) = \frac{1}{2}(1 + \sin 2\pi(x - \frac{5}{2}))e^{-50(x-\frac{1}{4})^2}, \quad |x| < 1,$$

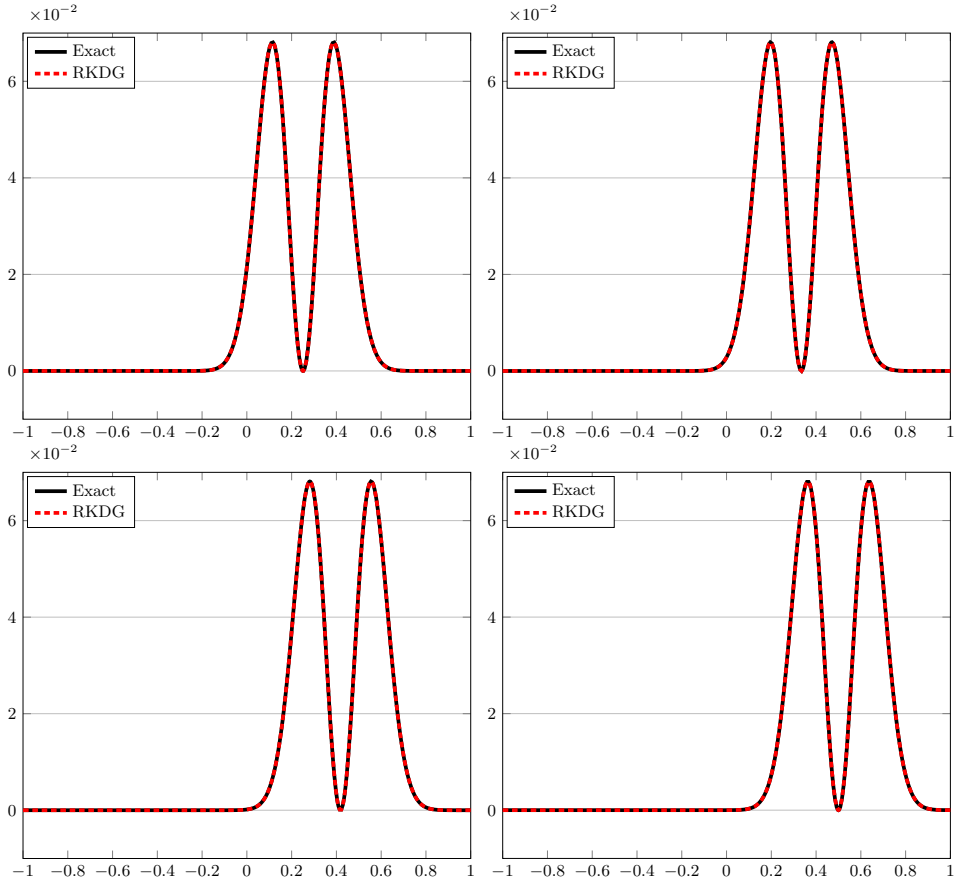

FIGURE 4. Numerical and exact solutions of Example 7.2 at time instants $t = \Delta t, 70\Delta t$ (top), and $t = 140\Delta t, 208\Delta t$ (bottom). In all plots, $k = 6$ and $N = 64$.

with parameters $a_L = a_R = 0.5$. *In this case, in view of the coupling condition* (2.3) *the exact solution of* (6.1) *is obtained by following the characteristics as follows*

$$u(x,t) = \begin{cases} u_0(x - a_L t), & x < 0, \\ \frac{a_L}{a_R} u_0(\frac{a_L}{a_R} x - a_L t), & 0 < x < a_R t, \\ u_0(x - a_R t), & x > a_R t. \end{cases}$$

In this example, we take $N = 64$ and $k = 6$. Based on these assumptions, we depict the numerical and exact solutions at different time instants $t = \Delta t, 70\Delta t, 140\Delta t$, and $t = 208\Delta t$ in Fig. 4. From Fig. 4, we can see that, the numerical solutions are in excellent agreement with the exact solutions. In an analogue way as for Example 7.1, the relative L_1, L_2, L_∞ norm errors versus time as well as the absolute errors at various time instants $t = s\Delta t, s = 1, 13, 26, \ldots, 195, 208$, are presented in the left and right of part of Fig. 5 respectively.

TABLE 1. Relative L_1-errors and the corresponding convergence rates for example 7.2 evaluated at time $t = T$ for $\Delta t = h/(2k+1)$ for different N and k.

	$k=0$		$k=1$		$k=2$		$k=3$		$k=4$	
N	E_1	order	E_1	order	E_1	order	E_1	order	E_1	order
16	9.00_{-3}	–	5.40_{-3}	–	7.10_{-4}	–	8.32_{-05}	–	3.86_{-05}	–
32	6.60_{-3}	0.45	1.18_{-3}	2.19	1.18_{-4}	2.59	9.90_{-06}	3.07	1.15_{-06}	5.07
64	5.21_{-3}	0.34	2.32_{-4}	2.35	1.36_{-5}	3.11	6.85_{-07}	3.85	9.21_{-08}	3.64
128	3.50_{-3}	0.57	5.44_{-5}	2.09	1.65_{-6}	3.05	4.91_{-08}	3.80	1.03_{-08}	3.16
256	2.10_{-3}	0.74	1.35_{-5}	2.01	2.03_{-7}	3.02	4.02_{-09}	3.61	1.27_{-09}	3.02
512	1.16_{-3}	0.85	3.38_{-6}	2.00	2.53_{-8}	3.01	4.20_{-10}	3.26	1.59_{-10}	3.00
1024	6.13_{-4}	0.92	8.45_{-7}	2.00	3.15_{-9}	3.00	4.73_{-11}	3.15	1.98_{-11}	3.00

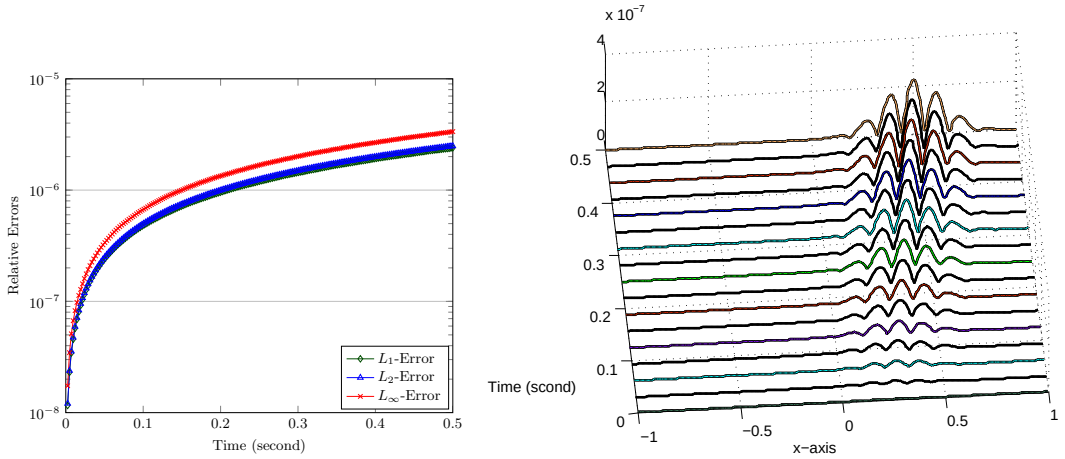

FIGURE 5. Relative L_2, L_1, and L_∞ errors versus t (left) and absolute errors at different time instants $t = s\Delta t, s = 1, 13, 26, \ldots, 195, 208$ (right) for Example 7.2. In both cases, $k = 6$ and $N = 64$.

In the next table we use different number of cells $N = 2^s$, for $s = 4, 5, \ldots, 10$ and measure the relative errors E_1 defined by (7.1) in the L_1-norm for various number of polynomial degrees $k = 0, 1, \cdots, 4$. These results that evaluated at time $t = T$ are presented in Table 1. Furthermore, the corresponding convergence rates are also reported in this table for a fixed k while then mesh size h is decreased. The numerical experiments shown in Table 1 indicate that achieving an order $(k+1)$ of accuracy is possible, if one uses the RKDG method with polynomials of degrees of $k = 0, 1, 2$. Of course, some inefficiencies are observed for the larger k, specially when the number of cells increased. The main reason for the inaccuracy is due to the

TABLE 2. Relative L_1-errors and the corresponding convergence rates for example 7.2 evaluated at time $t = T$ for $\Delta t = h/100$, $\Delta t = h^2$ for different N and $k = 3, 4$.

	$\Delta t = \frac{h}{100}$				$\Delta t = h^2$			
	$k = 3$		$k = 4$		$k = 3$		$k = 4$	
N	E_1	order	E_1	order	E_1	order	E_1	order
8	1.49_{-03}	–	5.14_{-04}	–	1.78_{-03}	–	8.72_{-04}	–
16	8.13_{-05}	4.20	3.56_{-05}	3.85	8.25_{-05}	4.43	3.98_{-05}	4.45
32	9.86_{-06}	3.04	8.25_{-07}	5.43	9.86_{-06}	3.06	8.64_{-07}	5.53
64	6.20_{-07}	3.99	2.57_{-08}	5.01	6.20_{-07}	3.99	2.62_{-08}	5.04
128	3.84_{-08}	4.01	8.15_{-10}	4.98	3.84_{-08}	4.01	8.20_{-10}	5.00
256	2.39_{-09}	4.01	2.55_{-11}	5.00	2.39_{-09}	4.01	2.55_{-11}	5.01
512	1.49_{-10}	4.00	8.15_{-13}	4.97	1.49_{-10}	4.00	7.86_{-13}	5.02

fact that the time-step is not optimal in the time marching algorithm. For instance, if instead of using the variable time-step $\Delta t = h/(2k+1)$, we utilize fixed time-steps $\Delta t = h/100$ as well as $\Delta t = h^2$, a significant better convergence rate is achieved for $k = 3, 4$ for various N in the L_1-norm. These experiments are shown in Table 2. Indeed, in the case $k = 4$ with the variable time-steps, the number of time levels used in the computations (Table 1) are $nt = 28, 36, \ldots, 1152, 2304$, while in the case of fixed time-steps $\Delta t = h/100$ we utilized $nt = 400, 800, \ldots, 12800, 25600$ (Table 2). On the other hand, in the case of $\Delta t = h^2$ we have to use $nt = 32, 128, 512, 2048, 8192, 32768$, and $nt = 131072$ number of time levels, see Table 2.

It can be seen from Table 2 that almost the same results are obtained if one utilizes two different fixed time-steps $\Delta t = h/100, h^2$, although the corresponding number of time levels are considerably different. This fact is also confirmed in Fig. 6 when we apply them to other values of $k = 0, 1, 2$.

Example 7.3 ($a_L < 0$, $a_R < 0$). *In the third example, we consider* (6.1) *with the initial condition*

$$u_0(x) = \begin{cases} 0, & |x| \geq 0.5, \\ -x - 0.5, & -0.5 \leq x < 0, \\ -x + 0.5, & 0 < x \leq 0.5, \end{cases}$$

which has obviously a discontinuity at the interface $x = 0$. Our parameters are taken as $a_L = a_R = -0.3$. Similar to the last example, by considering the coupling condition (2.3) *the exact solution of* (6.1) *becomes*

$$u(x,t) = \begin{cases} u_0(x - a_L t), & x < a_L t, \\ \frac{a_R}{a_L} u_0(\frac{a_R}{a_L} x - a_R t), & a_L t < x < 0, \\ u_0(x - a_R t), & x > 0. \end{cases}$$

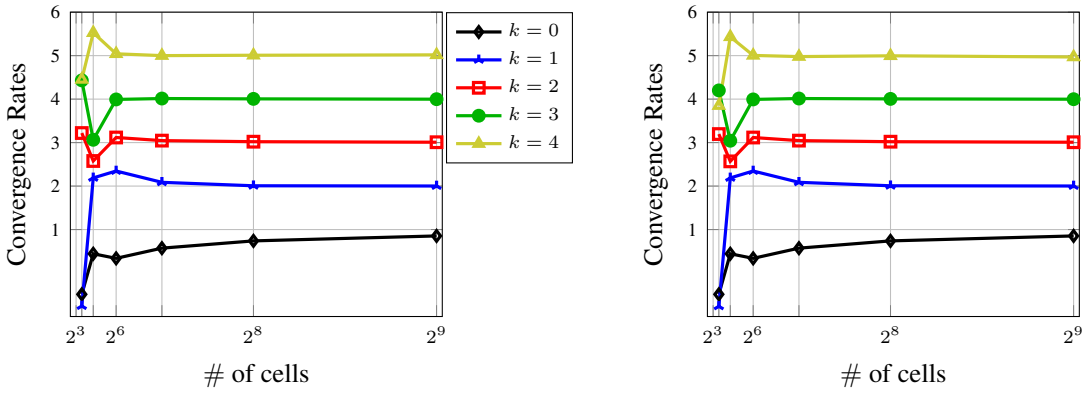

FIGURE 6. Convergence rates for example 7.2 using $\Delta t = h^2$ (left) and $\Delta t = h/100$ (right) evaluated at time $t = T$ for different $N = 8, \ldots, 512$ and $k = 0, 1, 2, 3$.

Firstly, we solve the problem with $k = 4$ on a uniform mesh with $N = 128$ number of cells. The snapshots of numerical solutions at different time instants $t = \Delta t, 96\Delta t, 192\Delta t$, and $t = T$ are displayed in Fig. 7. In all subplots, the exact solutions are shown by the solid lines. Obviously, the experiments in Fig. 7 for a fixed polynomial degree and number of cells indicate that the proposed scheme is stable even for a discontinuous initial condition and we observe only a slight oscillation near the discontinuity at $x = 0$.

In the next plot, we investigate the impact of different k in the RKDG scheme. The numerical solutions at time $t = T$ for different $k = 0, 1, 2, 3$ while the number of cells is $N = 64$, are presented in Fig. 8. Note that, to keep the number of time levels nt fixed for all k, we make use of $\Delta t = h/10$ instead of variable ones. Figure 8 can also be used for a comparison between the classical finite volume methods (FVM) which correspond to $k = 0$ and the higher order RKDG methods.

It can be clearly seen from Fig. 8 that how the finite volume approximation which represented by open circles, displaces the location of the discontinuity. As we expected, by increasing the degree of polynomials k, the obtained numerical solutions in Fig. 8 are get closer to the exact ones on the smooth regions and in particular in the vicinity of the discontinuity. However, they only oscillate near $x = 0$, where the jumps take placed. In other words, the RKDG method with capabilities of strong stability and optimal accuracy captures discontinuous jumps.

8. CONCLUSIONS

In this work, the Runge-Kutta discontinuous Galerkin methods for the coupling of two conservation laws is devised and implemented. The efficiency of the method proposed is demonstrated through numerical simulations. Theoretical analysis and numerical experiments show that the RKDG scheme is stable as well as accurate and exhibit a typical high-order behaviour in all proposed examples. In fact, one can achieve a $(k + 1)$th order of convergence rate when

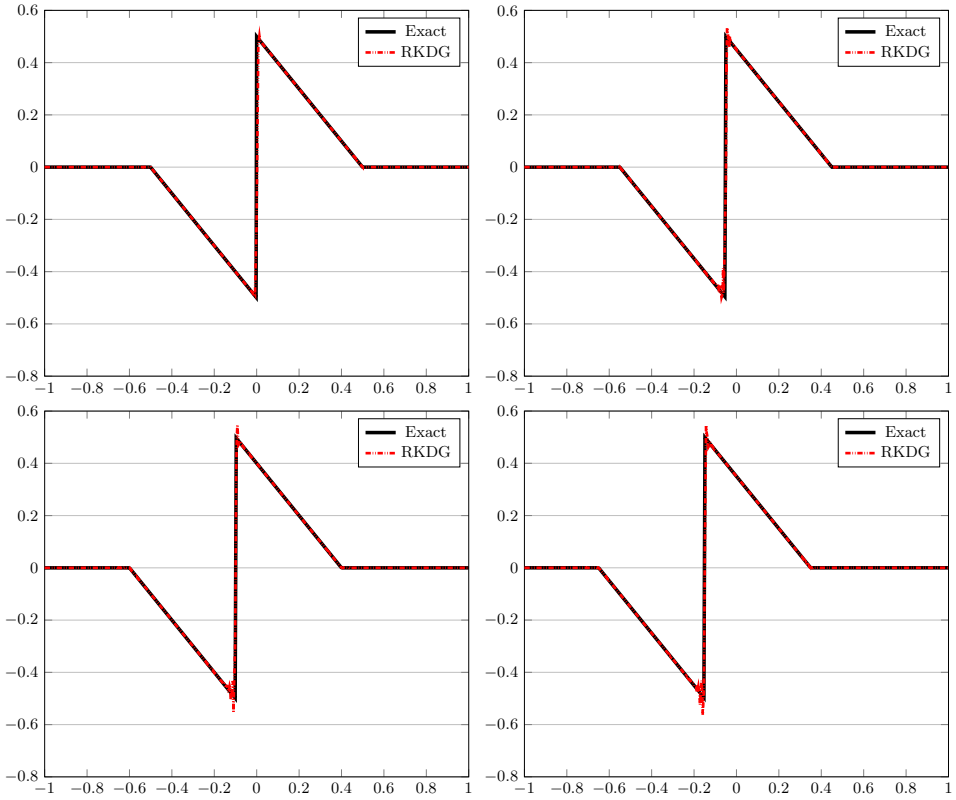

FIGURE 7. Numerical and exact solutions of Example 7.3 at time instants $t = \Delta t, 96\Delta t$ (top), and $t = 192\Delta t, 288\Delta t$ (bottom). In all plots, $k = 4$ and $N = 128$.

the special numerical upwind flux is utilized. For discontinuous solutions, it has the potential of sharply representing discontinuities. On the other hand, the finite volume results are much more smeared out and exhibited typical first-order behaviour.

In [32], the author proved a posteriori $L_2(L_2)$ and $L_\infty(H^{-1})$ residual based error estimates for a finite element method for the problem under consideration. Therefore, proving a posteriori error estimates of the DG schemes in any appropriate norm is worthy of future investigation. Moreover, the extension of this work to nonlinear and systems of conservation laws and also the impact of different numerical fluxes need further investigations.

REFERENCES

[1] E. Godlewski and P.-A. Raviart, The numerical interface coupling of nonlinear hyperbolic systems of conservation laws: I. the scalar case, Numer. Math., **97** (2004), 81–130.

[2] E. Godlewski, K.-C. Le Thanh, P.-A. Raviart, The numerical interface coupling of nonlinear hyperbolic systems of conservation laws: II. The system case, M2AN Math. Model. Numer. Anal., **39** (2005), 649–692.

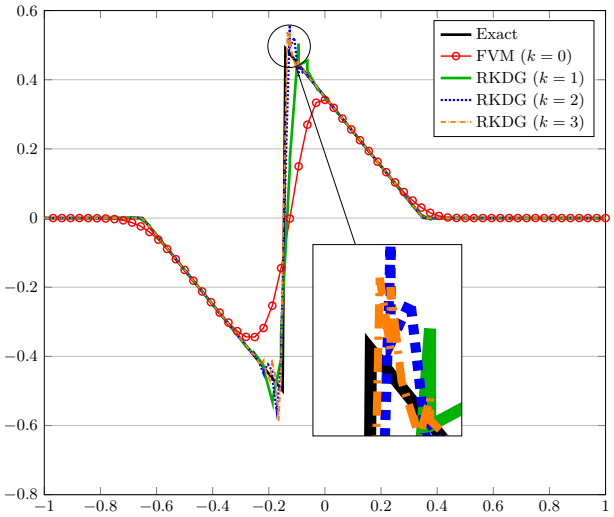

FIGURE 8. Comparison of numerical solutions at $t = T$ of Example 7.3 for $N = 64$, $\Delta t = h/10$, and various $k = 0, 1, 2, 3$. The solid curve corresponds to the exact solution and the magnification of solutions at discontinuous point $x = 0$ is plotted in the box.

[3] A. Ambroso, Ch. Chalons, F. Coquel, E. Godlewski, J.-M. Hérard, F. Lagoutière, P.-A. Raviart, and N. Seguin, The coupling of multiphase flow models, Proceedings of Nureth-11, Avignon, France, 2005.
[4] J.-M. Hérard, O. Hurisse, Coupling two and one-dimensional unsteady Euler equations through a thin interface, Computer and Fluids, **36** (2007), 651–666.
[5] A. Ambroso, Ch. Chalons, F. Coquel, E. Godlewski, J.-M. Hérard, F. Lagoutière, P.-A. Raviart, and N. Seguin, The coupling of homogeneous models for two-phase flows, Int. Journal for Finite Volume, **4** (2007), 1–39.
[6] A. Ambroso, Ch. Chalons, F. Coquel, E. Godlewski, J.-M. Hérard, F. Lagoutière, P.-A. Raviart, N. Seguin, and J.-M. Hérard, Coupling of multiphase flow models, Proceedings of the 11th international meeting on nuclear thermohydraulics, Nureth, 2005.
[7] F. Coquel, Coupling of nonlinear hyperbolic systems: A journey from mathematical to numerical issues, in Vázquez-Cendón et al. (Eds.), Numerical Methods for Hyperbolic Equations, Taylor & Francis Group, London, (2013), 21–35.
[8] B. Andreianov, K. H. Karlsen, and N. H. Risebro, A theory of L_1-dissipative solvers for scalar conservation laws with discontinuous flux, Arch. Rational Mech. Anal., **201** (2011), 27–86.
[9] R. Bürger, K. H. Karlsen, Conservation laws with discontinuous flux: a short introduction, J. Engrg. Math., **60** (2008), 241–247.
[10] R. Bürger, K.H. Karlsen, J. Towers, On Enquist-Osher-type scheme for conservation laws with discontinuous flux adapted to flux connections, SIAM J. Numer. Anal., **3** (2009), 1684–1712.
[11] S. Diehl, On scalar conservation laws with point source and discontinuous flux function, SIAM J. Math. Anal., **26** (1995), 1425–1451.
[12] K. H. Karlsen, N. H. Risebro, and J. D. Towers, Upwind difference approximations for degenerate parabolic convection-diffusion equations with a discontinuous coefficient, IMA J. Numer. Anal., **22**(4) (2004), 623–664.
[13] K.H. Karlsen, N.H. Risebro, J. D. Towers, L_1-stability for entropy solutions of nonlinear degenerate parabolic connection-diffusion equations with discontinuous coefficients, Skr.-K. Nor. Vidensk. Selsk. **3** (2003) 1–49.

[14] W.H. Reed and T.R. Hill, Triangular mesh methods for the neutron transport equation, Tech. Report LA-UR-73-479, Los Alamos Scientific Laboratory, Los Alamos, 1973.
[15] P. LeSaint, and P. A. Raviart, On a finite element method for solving the neutron transport equation, In de Boor, C. (Eds.), Mathematical Aspects of Finite Elements in Partial Differential Equations, Academic Press, (1974), 89–145.
[16] C. Johnson and J. Pitkäranta, An analysis of the discontinuous Galerkin method for a scalar hyperbolic equation, Math. Comp., **46** (1986), 1-26.
[17] T. Peterson, A note on the convergence of the discontinuous Galerkin method for a scalar hyperbolic equation, SIAM. J. Numer. Anal., **28** (1991), 133–140.
[18] G.R. Richter, An optimal-order error estimate for the discontinuous Galerkin method, Math. Comp., **50** (1988), 75–88.
[19] B. Cockburn, S. Hou, and C.W. Shu, The Runge-Kutta local projection discontinuous Galerkin method for conservation laws IV: the multidimensional case, Math. Comp., **54** (1990), 545–581.
[20] C.-W. Shu and S. Osher, Efficient implementation of essentially non-oscillatory shock-capturing schemes, J. Comput. Phys., **77** (1988), 439–471.
[21] B. Cockburn, C.-W. Shu, TVB Runge-Kutta local projection discontinuous Galerkin finite element method for scalar conservation laws II: General framework, Math. Comp., **52** (1989), 411-435.
[22] B. Cockburn, C.-W. Shu, TVB Runge-Kutta local projection discontinuous Galerkin finite element method for scalar conservation laws V: Multidimensional systems, J. Comput. Phys.,**141** (1998), 199–224.
[23] B. Cockburn, G.E. Karniadakis, and C. W. Shu (Eds.), Discontinuous Galerkin methods theory, computation and applications, Lecture Notes in Computational Science and Engineering, vol. 11, Springer, Berlin, 2000.
[24] J.S. Hesthaven, T. Warburton, Nodal Discontinuous Galerkin Methods: algorithms, analysis, and applications, Texts in Applied Mathematics, vol. 54, Springer Verlag, New York, USA, 2008.
[25] M. Izadi, Streamline diffusion methods for treating the coupling equations of two hyperbolic conservation laws, Math. Comput. Model., **45** (2007), 201–214.
[26] A. Vasseur, Strong traces for solutions of multidimensional scalar conservation laws. Arch. Ration. Mech. Anal., **160** (2001), 181–193.
[27] S.N. Kružkov, First order quasilinear equations in several independent variables, USSR Math. Sbornik. **10** (2) (1970) 217–243.
[28] Adimurthi and G. D. V. Gowda, Conservation laws with discontinuous flux, J. Math. Kyoto Univ., **43** (2003), 27–70.
[29] Y. Cheng, C.-W. Shu, Superconvergence of discontinuous Galerkin and local discontinuous Galerkin schemes for linear hyperbolic and convection-diffusion equations in one space dimension, SIAM J. Numer. Anal., **47** (2010), 4044–4072.
[30] S. Osher, Riemann solvers, the entropy condition, and difference approximations, SIAM. J. Numer. Anal., **21** (1984), 217–235.
[31] G. Jiang, C.-W. Shu, On a cell entropy inequality for discontinuous Galerkin methods, Math. Comput., **206** (1994), 531–538.
[32] M. Izadi, A posteriori error estimates for the coupling equations of scalar conservation laws, BIT Numer. Math., **49**(4) (2009), 697–720.
[33] M. Abramowitz, I.A. Stegun (Eds.), Handbook of Mathematical Functions, Dover, New York, 1965.
[34] S. Bertoluzza, S. Falletta, G. Russo, and C.-W. Shu, Numerical Solution of Partial Differential Equations, in: Advanced Courses in Mathematics, CRM, Barcelona, 2008.
[35] P.G. Ciarlet, The Finite Element Method for Elliptic Problems, Amesterdam, North Holland, 1987.
[36] B. Cockburn, C.-W, Shu, Runge-Kutta discontinuous Galerkin methods for convection-dominated problems, J. Sci. Comput., **16** (2001), 173–261.
[37] J.-M. Hérard, Schemes to couple flows between free and porous medium, Proceedings of AIAA (2005), 2005-4861.